Feedback between the Land Surface and Rainfall at Convective Length Scales

DOUGLAS B. CLARK AND CHRISTOPHER M. TAYLOR

CEH Wallingford, Oxfordshire, United Kingdom

ALAN J. THORPE

Department of Meteorology, University of Reading, Reading, United Kingdom

(Manuscript received 29 July 2003, in final form 24 December 2003)

ABSTRACT

The surface fluxes of heat and moisture in semiarid regions are sensitive to spatial variability of soil moisture caused by convective rainfall. Under conditions typical of the Sahel, this variability may persist for several days after a storm, during which time it modifies the overlying boundary layer. A model of the land surface is used to quantify the dependence of surface fluxes of heat and moisture on antecedent rainfall amount, time since rainfall, and surface properties. Next, a coupled model of the land and atmosphere is used to characterize the boundary layer variability that results from this surface variability, and its dependence on factors including the length scale of the surface variability. Finally, two- and three-dimensional modeling of squall lines is used to examine the sensitivity of rainfall to boundary layer variability. Boundary layer variability tends to be greater for surface variability on long length scales, but squall-line rainfall shows the strongest response for anomalies on small length scales, comparable to that of the convection. As a result, the feedback between soil moisture and rainfall will be strongest at an intermediate scale.

1. Introduction

Feedbacks between soil moisture and rainfall are thought to play an important role in determining the climate of many continental areas. Rainfall increases soil moisture and thus exerts a control on the surface fluxes of radiation, heat, and moisture back into the atmosphere. The amount and partition of these fluxes affect the properties of the planetary boundary layer (PBL), and, hence, the instability of the atmosphere to subsequent deep convection. The humidity of the atmosphere also directly affects mixing and microphysical processes involved in the growth of clouds and rainfall. These processes have been studied through both observations and numerical modeling. Betts and Ball (1998) analyzed observations over a grassland area and showed that the soil moisture state influenced PBL properties, while Findell and Eltahir (1999) concluded that the influence of soil moisture on near-surface air was at least partly responsible for a correlation between soil moisture and summertime rainfall in Illinois. Studies with large-scale numerical models have shown that the soil moisture affects the modeled climate and its temporal variability (e.g., Shukla and Mintz 1982; Delworth and Manabe 1989; Fennessy and Shukla 1999; Zeng et al. 1999; Pal and Eltahir 2001).

It is generally considered that such feedbacks operate at length scales of several tens of kilometers and upward, while shorter length scales have been much less studied. Indeed it has been argued that at shorter length scales advection and turbulence in the atmosphere would largely eliminate any coherent atmospheric anomalies associated with surface forcing (e.g., Shuttleworth 1988; Raupach 1991), thereby preventing any feedback between soil moisture and rainfall. The interaction of spatial variability of the land surface and moist convection has been the subject of several studies (e.g., Avissar and Liu 1996; Lynn et al. 1998), although these studies have tended to focus more on aspects such as the generation of mesoscale circulations and the initiation of convection rather than the full surface–atmosphere–rainfall feedback over several rain events. In a modeling study, Baker et al. (2001) noted that rainfall amounts were higher close to areas of wet soil and suggested that a positive feedback could result. Emori (1998) found from idealized modeling that the feedback between soil moisture and rainfall was negative because the spatially varying soil moisture generated mesoscale circulations that tended to initiate moist convection and rainfall over areas of dry soil. However, studies of rain gauge data from the African Sahel have suggested that a positive feedback mechanism was operating on a

Corresponding author address: D. B. Clark, CEH Wallingford, Crowmarsh Gifford, Oxfordshire OX10 8BB, United Kingdom.
E-mail: dbcl@ceh.ac.uk

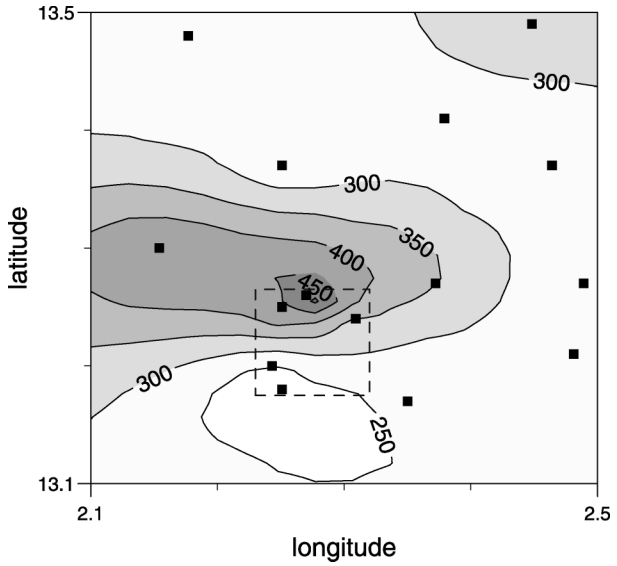

FIG. 1. Total rainfall (mm) for the period 31 Jul–18 Sep 1992 in the southwest of the HAPEX-Sahel study area. Rain gauges are denoted by squares, and the 10 km × 10 km area around the SSS is marked by a dashed line. Redrawn from Taylor et al. (1997).

length scale of some 10–20 km. Figure 1 shows rain gauge observations of rainfall from the Hydrological Atmospheric Pilot Experiment in the Sahel (HAPEX-Sahel; Goutorbe et al. 1997) in southwest Niger in 1992. Taylor et al. (1997) noted that the large rainfall gradient shown was the result of several storms over a 7-week period, but crucially each storm tended to rain more at the north of the Southern Super Site (SSS; a 10 km × 10 km area) than at the south. Such a pattern did not occur at this location in other months of the 1992 wet season, nor in other years, but Taylor and Lebel (1998) found that similar patterns had developed elsewhere in the area. Taylor et al. (1997) proposed that a land–atmosphere feedback was the cause of the persistent rainfall gradient. In this semiarid region, evaporation from the soil surface is an important component of the total evaporation, particularly in the few days immediately following rainfall. Spatial variability of rainfall leads to variability of soil moisture and soil evaporation, which in turn results in variability of the PBL. Observations of surface fluxes and near-surface and PBL properties supported this link. The final component of the proposed feedback loop was that convective cells, embedded in a storm, were preferentially enhanced at locations where the PBL was moister. This last part was studied by Clark et al. (2003, see also discussion in section 5 below) who used a numerical model to investigate the response of a squall line to idealized PBL variability and concluded that such local enhancements were possible.

The length scale of the proposed feedback, of the order of 10–20 km, is considerably smaller than has previously been studied. The question remains as to whether it is possible to get feedback between the land surface and rainfall at convective length scales, and if so, what controls its nature. The present work considers an idealized system in which all rain results from the periodic passage of large-scale storms, such as squall lines. (We use ''storm'' to refer to a weather system such as a squall line, while other authors may talk of smaller storms within a squall line.) This assumption is justified since squall lines and other mesoscale convective systems account for almost 90% of annual rainfall in the Sahel (D'Amato and Lebel 1998). Taylor and Lebel (1998) showed that these large storms favored the persistence of rainfall patterns. In this paper we examine the key processes that are required for a functioning feedback and examine how these vary with time and length scales. A numerical model is used to simulate typical Sahelian conditions. The examination focuses on the likelihood of feedbacks at small spatial scales. The next section introduces the numerical model used in this study, then section 3 describes the response of the land surface to rainfall. Section 4 examines the response of the PBL to surface variability, and section 5 looks at the sensitivity of squall lines to PBL variability, followed by the discussion in section 6.

2. Methodology and numerical model

In this study we used the Regional Atmospheric Modeling System (RAMS; Pielke et al. 1992) to simulate the land surface and atmosphere. The proposed land–atmosphere feedback was simulated in three steps: the response of the land surface to rainfall, the response of the PBL to rainfall-induced surface variability, and the response of a squall line to PBL variability. Splitting the study in this way allowed better examination of individual aspects of the feedback.

a. Modeling the land surface

In this first stage, the model was run in ''surface only'' mode at a single point for 1 week following a prescribed rainfall event, forced by observations of near-surface meteorology. This gave an estimate of the evolution of surface fluxes as the surface dried. The land surface in RAMS is represented by the Land Ecosystem–Atmosphere Feedback, Version 2 (LEAF-2) model of Walko et al. (2000). In brief, this simulates the energy balance of vegetation and bare soil, with evaporation coming from plant transpiration, intercepted water stored on the plant canopy, and bare soil. Soil temperature and moisture are modeled in each of 10 layers, down to 5.5 m. The model was forced by the mean diurnal cycle of temperature, humidity, wind speed, and radiation observed over the SSS for 4–14 September 1992, meaning that boundary layer feedbacks were neglected. The basic runs used parameter values for the fallow savannah, the validity of which has been confirmed through comparison of the model with observations by Taylor (2000). Values suitable for early September 1992 were used,

TABLE 1. Runs with the surface-only model. Each run was repeated for rainfall amounts of 0, 2, 5, 10, 20, and 30 mm, and these form a ''set.'' Runs within a set started from the same initial conditions. The observed profile of soil moisture refers to the 7 Sep 1992 case discussed in the text.

Set name	Vegetation fraction	LAI	Initial VSMC
Standard	0.30	0.65	Observed profile
Dry	0.30	0.65	0.03 at all depths
Wet	0.30	0.65	0.20 at all depths
Dense	0.95	2.00	Observed profile
Sparse	0.10	0.20	Observed profile
LAI	0.30	0.975	Observed profile

with a fractional coverage of vegetation of 0.3 and a leaf area index of 0.65. The root depth was 3.5 m, but 54% of the roots were in the topmost 0.24 m. A sandy soil type was used, with volumetric soil moisture content (VSMC) at saturation of 0.40 and a wilting point of 0.01. The initial soil moisture was as observed on 7 September 1992 with VSMC of approximately 0.05 close to the surface, increasing to approximately 0.1 at a 1.5-m depth. Transpiration is essentially unstressed when the VSMC is greater than 0.06 and was only weakly stressed by the observed VSMC. The relatively low VSMC is representative of conditions in a freely draining sandy soil a few days after rainfall. Each run was repeated for rainfall amounts (P) of 2, 5, 10, 20, and 30 mm, along with a run with no rain. Each set of runs thus consisted of six runs from the same initial conditions, the only difference being the amount of rainfall. The runs are described in Table 1. The Standard set refers to the fallow savannah vegetation and observed VSMC described above.

The runs were repeated for other soil moisture states. For the Dry set the initial VSMC was 0.03 at all depths, sufficiently dry to substantially restrict transpiration and crudely representative of a condition shortly after the start of the wet season, before the soil profile has wetted up. In the Wet set the initial VSMC was 0.2 at all depths. Table 1 also shows runs with different amounts of vegetation (sets Dense, Wet, and LAI). Although the description used in Standard is known to be a good representation of the SSS fallow savannah, runs with altered vegetation are for illustrative purposes only. The model was spun up for 1 day starting at 0000 local time (LT), then rainfall was applied during the first hour of the second day. Results are presented in section 3 and refer to the time since the canopy dried, so the interception loss was zero.

b. Modeling the PBL

The soil moisture and temperature from the surface-only runs were then used to provide the initial conditions for shorter runs of the model with both surface and atmosphere activated. These were used to assess the response of the PBL to spatial variability of the surface.

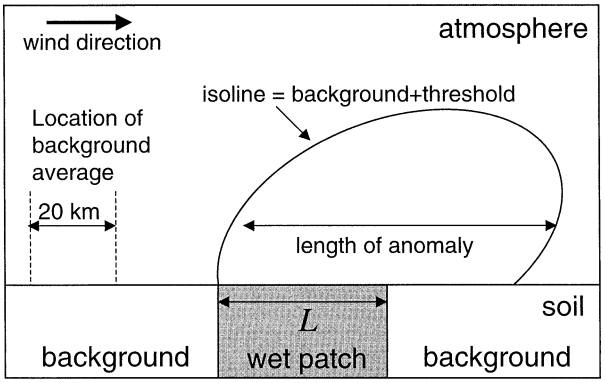

FIG. 2. Schematic of PBL experiment. The model was initialized with a patch of moist soil in an otherwise uniform background. Also shown are locations used in the definition of a PBL spatial anomaly. An anomaly was defined as an area where the field exceeded the background value by an amount at least equal to a threshold.

For this step RAMS was used in two-dimensional (z–x) mode, a simplification that allowed a large number of simulations. The domain size was 300 km in the horizontal, with a cyclic lateral boundary condition and a grid-box size of 1 km. In the vertical there were 66 levels extending to over 10 km, with the first level at 11-m height and 23 levels in the lowest 1 km. Radiation was parameterized following Chen and Cotton (1983), and moisture was not allowed to condense. Subgrid turbulent mixing was represented by a first-order deformation parameterization, with coefficients from McNider and Pielke (1981). The initial atmospheric temperature and humidity were based on the HAPEX-Sahel radiosonde ascent for 0730 LT on 2 September 1992 (Dolman et al. 1997), while the initial wind was constant with height. Surface characteristics were for the fallow savannah, as before, except where stated otherwise.

An area of wet soil, of length L, was added to an otherwise uniform background condition (see Fig. 2). The soil in the wet patch was initialized using results from a surface-only run in which rainfall amount was denoted P_w, while the background soil conditions were set from a run in which the rainfall was P_b. For any value of P_w or P_b, the soil conditions in the surface-only runs were a function of the time since rainfall (T). Thus for each pair of values for P_w and P_b there were five PBL runs starting from different soil conditions, corresponding to $T = 1, 2, 3, 4$, or 5 days. A reference set of runs (REF) used $L = 20$ km, $P_w = 30$ mm, $P_b = 0$ mm, and initial wind speed (u) of 3 m s^{-1}. The runs are summarized in Table 2. Sets RAIN and BACK investigated the effect of changing the wetness of the wet patch and background, respectively. DRY considered a generally drier soil state, while the set LAI increased the leaf area index in the wet patch. WIND and LENGTH investigated the effects of varying u and L, respectively.

As far as the present study is concerned, surface-induced spatial variability of the PBL is primarily

TABLE 2. Runs with the coupled surface–atmosphere model. Each run was repeated using initial conditions for $T = 1, 2, 3, 4, 5$ days to form the given sets.

Set name	Surface and soil conditions (name of set in Table 1)		Antecedent rainfall (mm)		Length of wet patch, L (km)	Initial wind speed, u (m s^{-1})
	Wet patch	Background	Wet patch (P_w)	Background (P_b)		
REF	Standard	Standard	30	0	20	3
RAIN	Standard	Standard	5, 10, 20, 30	0	20	3
BACK	Standard	Standard	30	5, 10, 20	20	3
DRY	Dry	Dry	30	0	20	3
LAI	LAI	Standard	30	0	20	3
WIND	Standard	Standard	30	0	20	1–10
LENGTH	Standard	Standard	30	0	5–50	3

caused by spatial variability in the surface fluxes of heat and moisture. At night these fluxes are small and advection will tend to remove any PBL variability. It was assumed that early in the morning there was negligible PBL variability, and a horizontally homogeneous atmosphere was specified at 0700 LT. The same initial profiles of atmospheric temperature and humidity were used in all runs, whereas in reality these fields evolve from day to day. PBL variability is also affected by atmospheric advection associated with larger-scale weather systems that are not represented here.

Since water was not allowed to condense, moist convection and rainfall could not occur in the PBL runs. This simplification was consistent with the aim of studying the possible feedback between soil moisture and large-scale storms. In this particular section, the aim was not to study the initiation of convection or squall lines, but to model the development of PBL variability in the days between storms. This PBL variability may then affect the rainfall pattern from the next storm that propagates through the study area (which is considered below). This study has not considered rainfall from isolated convection, since the majority of rainfall in the Sahel comes from large-scale storms (see the introduction). In this environment the impact of isolated convection may well be of secondary importance to the development of a feedback loop.

With these assumptions the experiment was able to address the extent to which a heterogeneous surface was able to generate spatial variability in the atmosphere at various stages as it dried. The results of this section of work are discussed in section 4.

c. Modeling a squall line

In the final stage, the response of a squall line to idealized PBL variability was assessed using three-dimensional simulations. The overall approach was the same as that used by Clark et al. (2003). It was not possible to investigate the squall line's response to the modeled PBL variability based on the 2 September 1992 profile described above because the model did not support a storm in that environment. No squall line occurred on that day and even given an environment in which a squall line is known to have occurred, a model may fail to sustain a squall line for various reasons, including deficiencies in the model. Instead, the initial atmospheric profile was based on the sounding ahead of the 23 June 1981 squall line in the Ivory Coast used by Caniaux et al. (1994). A Galilean transformation was applied to the wind field to keep the storm centered in the grid. The along-line component of the wind was set to zero for consistency with the results of Clark et al. (2003), although the direction of vertical wind shear is known to affect the nature of storms (e.g., Weisman et al. 1988). The horizontal domain of RAMS was set to 250 km in the direction of squall-line movement (the x direction) and 75 km in the along-line direction (the y direction). A radiative boundary condition was used in x, and a cyclic condition in y. This 75-km length is a multiple of the 25-km autocorrelation length in the along-line direction reported by Redelsperger and Lafore (1988) from radar data. The assumption of periodicity in the along-line direction has been used by several studies, including Nicholls and Weissbluth (1988). The grid covered 20 km in the vertical with the spacing of grid points increasing from 104 m in the lowest layer to 1 km above 12-km height. Radiation and surface fluxes were neglected in this stage, as previous studies have suggested that they do not play a major role in short-term simulations of squall lines (e.g., Redelsperger et al. 2000), while six species of condensate were modeled following Walko et al. (1995).

A squall line was initiated by prescribing a cooling over the first 10 min. The basic cooling was constant in the y direction and pseudorandom noise was added to generate along-line variability. The modeled convection was initially linear and became more fully three-dimensional with time. Results presented here refer to times around 2 h after initiation when the convection was in transition toward becoming fully 3D. Fully 3D convection is highly variable in space and, whereas Clark et al. (2003) could generate ensembles of 2D runs to sample this variability, such an approach in 3D was beyond the resources of this project. By considering relatively early times in the simulations, the experiment was made more manageable, while a more comprehensive study will be possible in the future. Following Clark

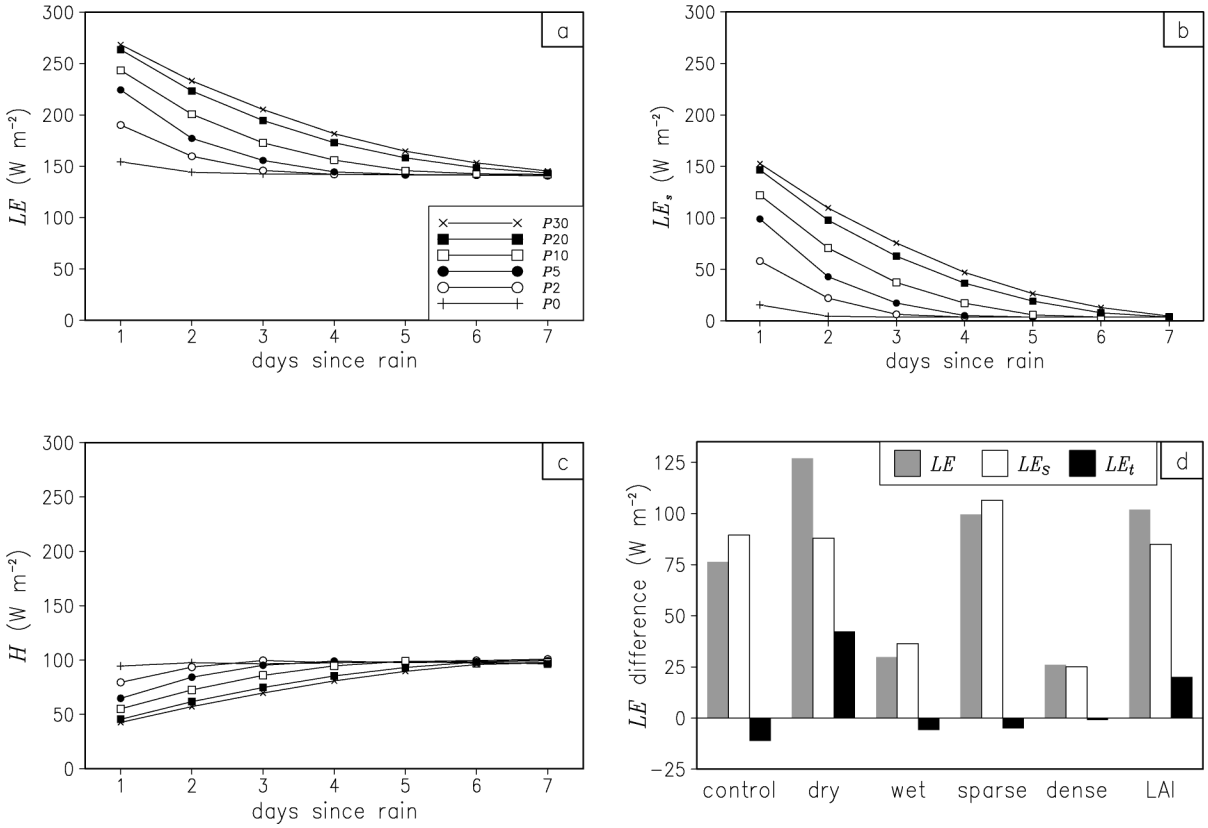

FIG. 3. Daytime average surface fluxes (W m^{-2}). The effect of different rainfall amounts (P) as a function of days since rain, for the CONTROL set of runs: (a) total latent heat, (b) bare soil latent heat, and (c) sensible heat. (d) The effect of initial soil moisture and vegetation type. The plotted values are differences of total latent heat flux, bare soil latent heat flux, and transpiration between runs with $P = 30$ and $P = 0$ mm, averaged over days 1–4.

et al. (2003), idealized PBL variability was represented by humidity anomalies added ahead of the squall line. Results from this section of work are described in section 5.

3. The response of the land surface to precipitation

The evolution of the surface energy budget in the days following rainfall was studied for rainfall events of different size, with particular emphasis on the persistence of enhanced evaporation. The model was configured as described in section 2a. Various components of the surface energy balance for the runs in the Standard set are shown in Fig. 3. Values plotted are averages over 0600–1800 LT, hereafter called daytime averages. Each figure shows the variation over the 7 days following rainfall amounts of 2, 5, 10, 20, and 30 mm, in addition to a run without rain. Figure 3a shows large differences of evaporation over the days immediately following rainfall, with larger differences persisting longer for larger P. Note that a daytime average latent heat flux (LE) of 100 W m^{-2} corresponds to 1.7 mm of evaporation. These differences of LE were primarily because of differences in the latent heat flux from the soil surface LE_s (Fig. 3b). The time taken to relax back to the $P = 0$ line depends upon the time for the extra soil moisture to be diminished by LE_s and drainage to deeper soil layers. Transpiration (LE_t; not shown) varied by less than 20 W m^{-2} across the whole period, largely as a decrease on days 1 and 2 when LE_s was large. There was relatively little difference in the surface energy balance between runs with $P > 20$ mm, because the top soil layer was saturated and any more rainfall drained to deeper levels.

Changes in sensible heat flux H (Fig. 3c) were of opposite sign to those of LE and of magnitude less than half those of LE (at least over the first few days when differences were substantial). Net radiation R_n increased immediately after rainfall (not shown), primarily because of less longwave emission from a cooler surface but also because of the lower albedo of the wet soil. However, for all $P > 0$, the increase of LE was greater than that of R_n and so H decreased.

Figure 3 implies that spatial variability of rainfall can lead to substantial variability of the surface energy budget for some 3 days or so after rainfall, for the fallow savannah. For example, 2 days after rain, a location with

$P = 30$ mm would have daytime-average LE 56 W m^{-2} greater than a location where $P = 5$ mm, assuming the same conditions at the reference level. Such variability could have a substantial impact on the atmosphere, depending upon other conditions such as the length scale of the variation. This is investigated in section 4.

The initial soil moisture profile is also important in determining the flux difference between two points. Figure 3d compares the daytime average difference of LE between $P = 30$ mm and $P = 0$ mm, averaged over the first 4 days following rainfall. The values shown for the Standard case are the time-averaged difference between $P = 30$ and $P = 0$ in Fig. 3a. For the Dry and Standard cases, LE_s is similar since it is primarily controlled by the rainfall amount; however, the total LE differs because the background soil moisture in Dry is insufficient to maintain transpiration in the absence of rainfall ($P = 0$). In contrast, for the Standard and Wet cases there is little difference in transpiration since this is unstressed by soil moisture in both; instead, the difference is the result of LE_s, which declines less rapidly in all Wet cases because of the high initial VSMC. Thus given the same spatial distribution of rainfall depths, the spatial variability of LE is generally greater given drier antecedent conditions.

The effect of varying the amount of vegetation is also represented in Fig. 3d. In general, sparser vegetation increases the influence of bare soil evaporation on the overall surface energy budget. As the persistence of evaporation anomalies is closely linked to bare soil (Fig. 3b), the density of vegetation is an important control on any persistence. Figure 3d confirms that sparser vegetation (SPARSE) increased the variability of LE_s and LE, while denser vegetation (DENSE) had the opposite effect. There are large areas of the Sahel, including agricultural areas growing millet, where the vegetation is indeed less dense than the standard case of fallow savannah used here and where rainfall-induced spatial variability may be enhanced. A feedback not considered so far is the influence of soil moisture on the development of leaf area. There is some evidence that leaf area is increased in areas of persistently higher soil moisture; indeed Taylor (2000) considered that this was the dominant cause of spatial variability of evaporation after 4 or 5 days without rainfall. The LAI case in Fig. 3d shows that enhanced leaf area index in the wet patch increases the evaporation difference over the standard case, primarily through transpiration.

In summary, rainfall exerts a powerful control on evaporation from the sparsely vegetated Sahelian land surface in the days immediately following a storm. Spatial variability of rainfall of the order of 20 mm, such as is common within convective storms, results in substantial spatial variability of surface fluxes.

4. The response of the boundary layer to surface variability

The next stage of the investigation examined the impact of spatial variability of the surface on the PBL, using the model as described in section 2b. To recap, a patch of wet soil was introduced in an otherwise uniform background condition, and the model was then integrated over the diurnal cycle. These initial soil conditions were taken from surface-only runs. By varying the time in the surface-only run at which the soil conditions were extracted, the drying of the soil over the days following rainfall was represented in the PBL runs. In addition to studying the effect on the PBL of different amounts of rainfall-induced surface variability, we also examined the effects of the length scale of the surface variability and the background wind speed. In the following sections we first describe the diurnal evolution of the modeled PBL, then consider spatial variability of the PBL.

The initial profiles of atmospheric potential temperature and humidity in the lower atmosphere are presented in Fig. 4a, while the diurnal evolution of selected PBL properties are shown in Figs. 4b and 4c for the run in REF with $T = 2$ days. These are background average values, defined as a 20-km average well upwind of the moist patch where there is negligible effect of the patch. Figure 4b shows that the PBL deepened and warmed throughout the day until early evening. The water vapor mixing ratio (r_v) in the PBL decreased slightly through most of the day (Fig. 4c) because although water was input from surface evaporation, the PBL was deepening and drier air was entrained from above. However, the increasing depth of the PBL meant that the precipitable water content (W) of the PBL increased.

Below we discuss the magnitude of PBL spatial variability in a range of model runs. The variability is quantified in terms of atmospheric anomalies, with an anomaly defined as a value that exceeds the background value by an amount greater than a threshold (see also Fig. 2). The background value varies in time (and to a lesser extent between runs), and the anomaly is a measure of the spatial variability at any given time. Later sections necessarily use summary statistics, such as the daily maximum anomaly, but first we set these values in the context of the diurnal cycle by considering the evolution of anomalies in run REF with $T = 2$ days. Spatial anomalies of PBL-average r_v and W are shown in Fig. 4d. The anomalies were defined using hourly averaged data, and both the mean anomaly and the maximum point value are plotted. The anomalies show a similar diurnal course, regardless of the variable or the measure used, with a maximum at around 1700 LT. The timing of the maximum reflects the balance of input by surface evaporation versus extraction by entrainment and advection, combined with changes in PBL depth. In most of what follows we use the maximum W anomaly to quantify the strength of atmospheric variability, with a threshold value of 0.15 mm. As noted above, alternative measures generally show similar behavior. Alternative thresholds only changed the quantitative details of the results, not the qualitative nature. A threshold greater than zero was

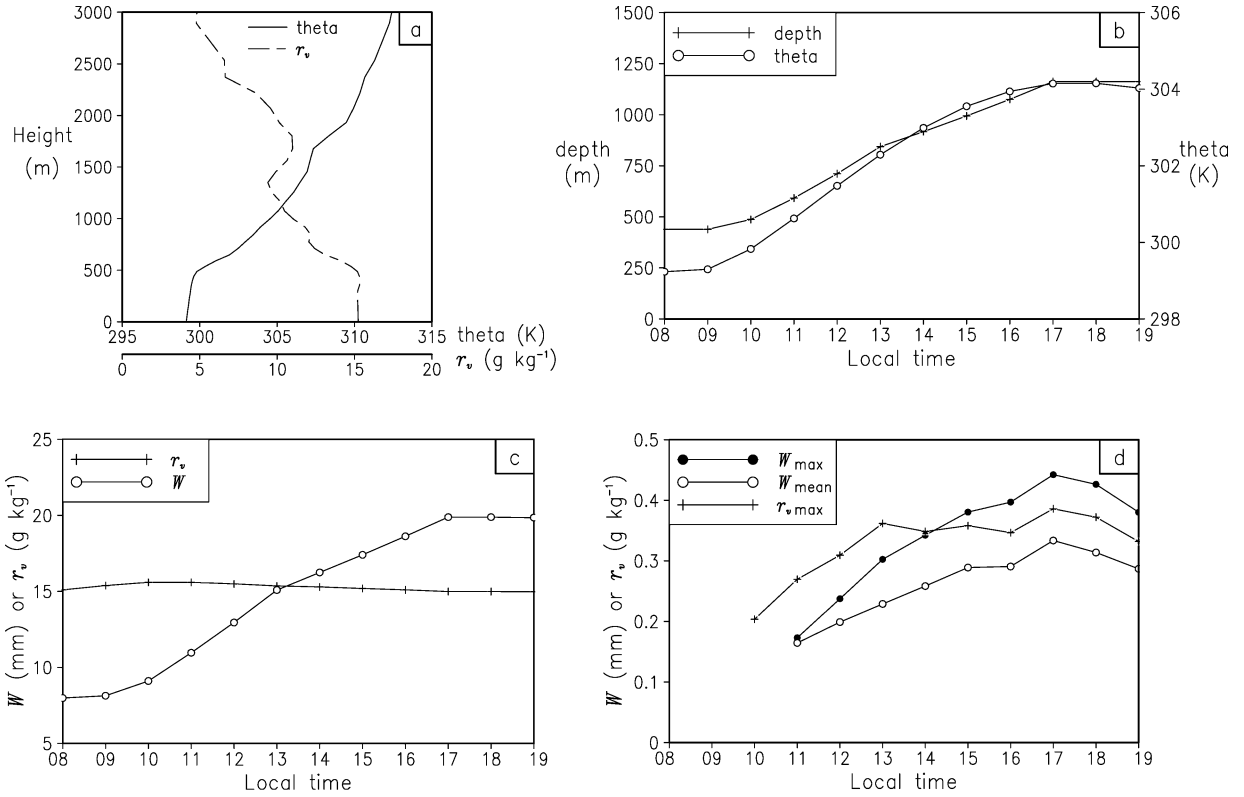

FIG. 4. Initial atmospheric profiles and the diurnal evolution of PBL properties for the run in REF with $T = 2$ days. (a) Initial potential temperature (theta; K) and humidity mixing ratio (g kg^{-1}) in the lower atmosphere. Time series of hourly mean quantities: (b) depth of PBL (m) and vertically averaged PBL potential temperature (K), (c) vertically averaged PBL humidity mixing ratio (g kg^{-1}) and precipitable water (mm), and (d) spatial anomalies of vertically averaged PBL humidity mixing ratio (g kg^{-1}) and precipitable water (mm). For each hour the maximum point anomaly is shown for mixing ratio and precipitable water, and the mean anomaly is also shown for precipitable water. Anomalies less than 0.15 g kg^{-1} or 0.15 mm are not plotted.

necessary to exclude small changes at the edge of diffuse features.

a. Sensitivity to surface conditions

The magnitude of any anomaly varies with the magnitude of surface flux spatial variability, which is a function of both antecedent rainfall variability and the time since rainfall. These effects are summarized in Fig. 5 for experiment RAIN. The smallest rainfall contrast resulted in a relatively modest PBL anomaly on the first day only, and after that there was insufficient spatial variability of surface fluxes to generate significant variability in the PBL. Larger rainfall contrasts produced a PBL anomaly for 3 or 4 days after the rain event. The assumption of zero background rainfall ($P_b = 0$) in RAIN is the extreme case, but results for $P_b > 0$ (set BACK; not shown) tend toward the $P_b = 0$ case with time, as the drier patch dries out, so that, for example, after 2 days there is relatively little difference between $P_b = 5$ mm and $P_b = 0$ mm. This is consistent with the trend to less variability of surface fluxes seen in Fig. 3.

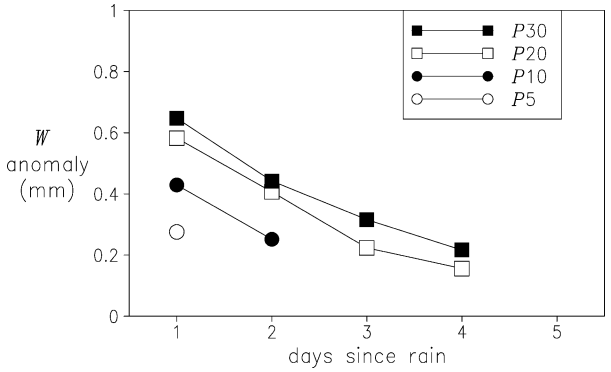

FIG. 5. Maximum hourly spatial anomaly of PBL precipitable water (mm) as a function of days since rain, for runs in set RAIN. Values are shown for wet patch rainfall of 5, 10, 20, and 30 mm.

In section 3 it was shown that surface flux variability was sensitive to antecedent soil moisture and vegetation density, and model runs DRY and LAI (not shown) confirmed that this also affected PBL spatial anomalies. The maximum W anomaly, averaged over $T = 1$–4 days, was 205% of the RAIN value for DRY, and 151% for LAI. Furthermore, both scenarios showed substantial PBL variability up to 6 days after rain.

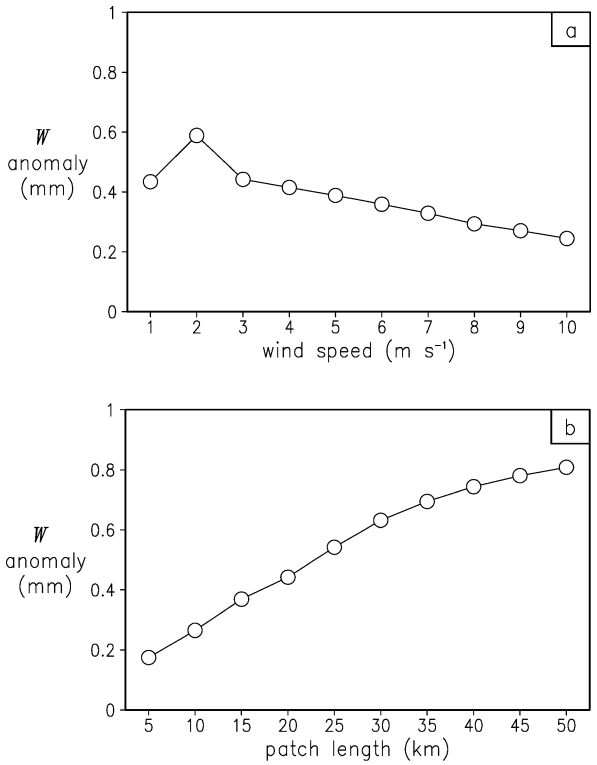

FIG. 6. Maximum hourly spatial anomaly of PBL precipitable water (mm) as a function of (a) wind speed (m s^{-1}) and (b) wet patch length (km). Data are from sets WIND and LENGTH.

b. Effect of length scale and wind speed

The spatial anomaly is also affected by the length of the wet patch and the initial wind speed, as summarized in Fig. 6. Figure 6a shows the effect of varying u from 1 to 10 m s^{-1} with $L = 20$ km (set WIND). The strength of the anomaly decreases roughly linearly with $u > 2$ m s^{-1} and is a maximum for $u = 2$ m s^{-1}. The smaller anomaly at 1 m s^{-1} was a result of a relatively strong mesoscale circulation in these light wind conditions that altered the development of the anomaly (further details in section 4d). Figure 6b shows the effect of varying L from 5 to 50 km, with $u = 3$ m s^{-1} (set LENGTH). The maximum anomaly became larger as the patch length increased because of the decreasing effect of diffusion and advection. The rate of increase declined with increasing length scale and the humidity values within large patches approach those over a uniformly wet surface. The effects of advection, diffusion, and entrainment controlled the extent to which the PBL anomalies differed from those calculated from the spatial variability of modeled evaporation. In any of the runs shown in Fig. 6b, the difference of evaporation between dry and wet points over the 10 h from 0700 LT to the typical time of maximum PBL anomaly at 1700 LT was equivalent to approximately 1.0 mm of evaporation. For large length scale patches, Fig. 6b shows values that are approaching this, minus an amount for entrainment, while over shorter patches advection is clearly important in reducing the PBL anomaly.

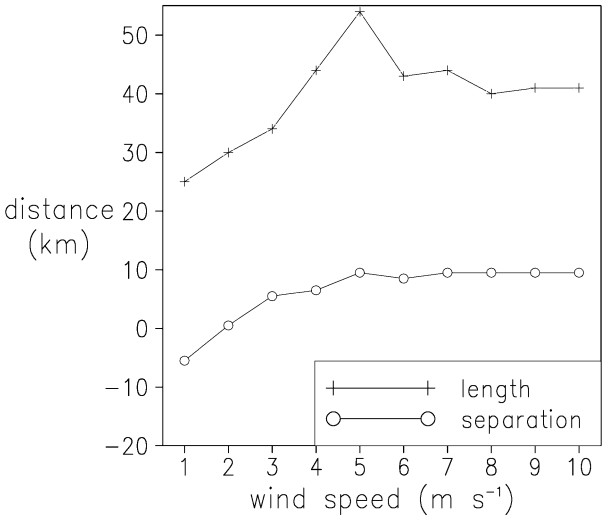

FIG. 7. Length and location (km) of spatial anomaly of precipitable water for runs in set WIND. Values are the length with anomaly >0.15 mm, and the separation between the location of maximum anomaly and the center of surface patch.

The length of the atmospheric anomaly and its location relative to the surface wet patch also varied with u and L. In nearly all cases the maximum PBL anomaly occurred 0–10 km downwind of the center of the surface patch (Fig. 7 shows this for the WIND set) and in all cases this was over the surface patch. For the WIND set, Fig. 7 shows that the length of the W anomaly above a 0.15-mm threshold was approximately equal to L in light winds, but increased to over 40 km for $u = 5$ m s^{-1}. Beyond this the anomaly length decreased because stronger winds generally resulted in a smaller magnitude anomaly, less of which exceeded the threshold. The length of the anomaly is clearly sensitive to the threshold value used to define an anomaly. Using an alternative threshold of 75% of the maximum point anomaly, most runs gave an anomaly length in the range 20–30 km. For LENGTH, there was an approximately linear relationship between L and the length of the PBL anomaly (not shown), with the anomaly being 7 to 13 km larger than L (11 km larger on average).

The precise values used to describe the complicated shape of the anomaly plume were sensitive to thresholds, but the variation of the strength and size of the anomaly can be summarized qualitatively. Stronger winds tended to produce weaker, more diffuse anomalies that were shifted downwind, but the maximum anomaly remained over the surface patch. The length of the PBL anomaly tended to be larger than that of the surface feature, substantially so in cases of moderate wind, but there was less difference in light winds.

c. Thermodynamic indicators

Moist convection is sensitive to both the temperature and humidity of the PBL. In section 3 it was noted that

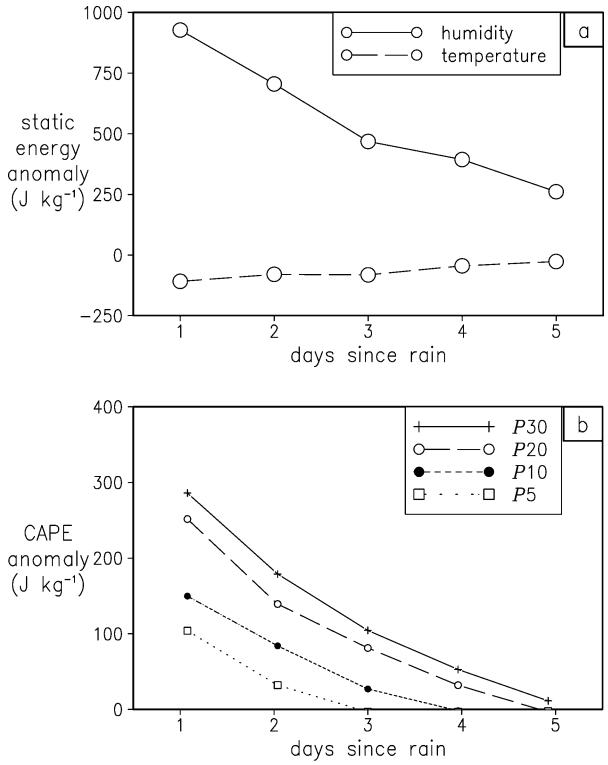

FIG. 8. PBL spatial anomalies as a function of days since rain for runs in set RAIN. (a) Contributions to moist static energy anomaly (J kg^{-1}) from humidity and temperature anomalies. Values are maximum hourly values of vertically averaged anomalies. Values were further averaged over the extent of the humidity anomaly. Wet patch rainfall was 30 mm. (b) Anomalies of CAPE (J kg^{-1}) for runs with a variety of wet patch rainfall amounts. Anomalies of precipitable water for these runs are shown in Fig. 5.

anomalies of H were of smaller magnitude than those of LE. Furthermore an atmospheric temperature anomaly elicits a dynamical response that tends to remove the anomaly. Both effects tend to reduce the variability of temperature in comparison with that of humidity. The relative importance of anomalies of humidity and temperature can be compared in terms of moist static energy (MSE), which for present purposes can be defined as $c_pT + L_vr_v + gz$, where c_p is the heat capacity of air at constant pressure, T is temperature, L_v is the latent heat of vaporization, g is the acceleration due to gravity, and z is height. Larger values of MSE in the lower atmosphere tend to be associated with stronger moist convection. Figure 8a compares the contributions to MSE from humidity and temperature anomalies for REF and shows that humidity variations were much more important. The average ratio of the anomalies of humidity to those of temperature for the runs shown in Fig. 8a was -3.4 g kg^{-1} K^{-1}, and as $L_v/c_p \approx 2500$ K the humidity anomalies are further emphasized.

Thermodynamic measures, such as the convective available potential energy (CAPE), are often used as an index of storm strength. Figure 8b provides an estimate of spatial anomalies of CAPE for the same runs. CAPE was calculated from hourly average profiles at the time and location of the maximum W anomaly. The plotted values are CAPE for a parcel with properties given by the average of the lowest 500 m. There was a strong diurnal cycle of the background CAPE (not shown), similar to those seen in other PBL quantities (Fig. 4), with an early morning minimum and a maximum in the afternoon convective boundary layer, but again there was little variation of the background field between days. Hence at the time of maximum W anomaly, background CAPE was relatively constant from day to day at approximately 1670 J kg^{-1}, and the anomalies shown in Fig. 8a were due to moist conditions over the wet patch. The anomalies indicated for $P_w = 30$ mm represented 17%, 11%, and 6% changes on days 1, 2, and 3, respectively. Convective cells in a Sahelian squall line are initiated when low-level air is forced to ascend above its level of free convection (LFC) by the advancing cold pool (e.g., Roux et al. 1984). For this forced convection, the convective inhibition (CIN) is not important. The increased CAPE over the wet patch was the result of a lower LFC and extra buoyancy of ascending parcels because of increased low-level humidity. The experiments analyzed here were based on a single initial atmospheric profile, and nonlinear measures such as CAPE cannot easily be extrapolated to other conditions. However, fractional changes of this size would be expected to produce substantially stronger convection in a squall line.

d. Effect of atmospheric initial condition and further discussion

A further set of experiments was performed for nine other initial atmospheric profiles, based on the days in late August and early September 1992 for which HAPEX-Sahel radiosonde ascents were made at approximately 0700 LT. The 2 September profile that was used in the bulk of this work was chosen because it represented a moderate case in terms of resultant PBL anomalies. In particular, for run REF with $T = 2$ days that gave a maximum point W anomaly of 0.44 mm, the nine cases ranged from 0.37 to 0.58 mm, while the maximum mean anomaly ranged from 0.28 to 0.36 mm with 0.34 mm in REF. The range was thus fairly modest, although it is not known how representative these profiles were of the wet season as a whole. Sensitivity experiments in which the initial profile was arbitrarily altered demonstrated that greater spatial variability of PBL humidity mixing ratio occurred if the PBL was shallow, so that surface flux variability was mixed through a smaller depth. This is an example of conditions that might engender greater PBL variability than was modeled above.

The modeled spatial variability of surface heating tended to induce weak mesoscale circulations, with the strength of the circulation being greater in conditions of light background wind. The general pattern was of

descent over the surface wet patch flanked by ascent at both edges, with the intensity of the circulation increasing until early evening. Descent over the wet patch tended to slow PBL growth and hence increased the magnitude of PBL anomalies because the surface flux was mixed through a shallower depth. In contrast, smaller PBL anomalies resulted in some runs when the descending dry air over the surface wet patch effectively split the PBL humidity anomaly into two. One part remained over the wet patch, while the other was advected downwind (the smaller anomaly seen in Fig. 6a for $u = 1\ \mathrm{m\ s^{-1}}$ was caused by such an event). The former was stronger because of greater surface evaporation over the wet patch and so was sampled for all statistics presented above, but it is clear that the structure of the PBL can become much more complicated than a single, well-defined anomaly. An analysis of the details of time-varying mesoscale circulations would constitute a separate study.

This section has shown how spatial variability of surface fluxes results in variability of the PBL. This part of the proposed feedback would favor feedback at relatively long length scales where advection and diffusion have less effect and would operate only if storms propagated through the area of the feedback at least once every 3 days or so, when spatial variability of the PBL can be large.

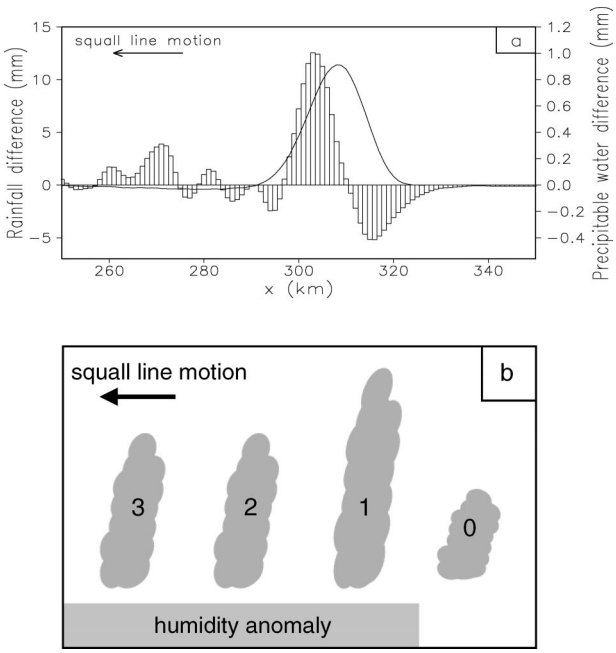

FIG. 9. (a) Ensemble mean difference of rainfall (mm; bars) and prescribed difference of column precipitable water (mm; line) in two-dimensional simulations. The difference is relative to the control ensemble. Redrawn from Clark et al. (2003). (b) Schematic of the mechanism. Four convective cells in a multicellular squall line are shown. The cells are consecutive in time, with the most recent cell on the left. See text for details.

5. The response of a squall line to boundary layer variability

Previous sections have considered how rainfall affects the land surface and the PBL. In this section we consider the final part of the proposed feedback loop, namely, the sensitivity of rainfall from a squall line to variability of PBL humidity. We start by summarizing the basic characteristics of squall lines and the results of two-dimensional experiments that were analyzed in detail by Clark et al. (2003) and then describe further experiments with the three-dimensional model.

a. Background

A mature squall line typically has a pool of cold air at the surface that forces warm, moist boundary layer air to rise, causing water vapor to condense and form deep clouds (convective cells) that move back relative to the gust front at the head of the cold pool. Mature squalls are often in a ''quasi-steady'' state in that these new clouds are regularly formed at the gust front, although the individual cells are relatively short-lived. Several cells at various stages in their life cycle often exist at a given time, with the newest cell closest to the front of the system and older cells toward the rear, and the system is called a multicellular squall line. For further details of squall-line dynamics, see Houze (1993).

Clark et al. (2003) studied the response of simulated two-dimensional squall lines to idealized variability of humidity. Humidity anomalies of various lengths were introduced to the lowest 1 km of the atmosphere ahead of a mature squall line, and ensembles of simulations were created to better account for the large stochastic element in the appearance of convective cells. Figure 9a shows the ensemble mean rainfall response from one such experiment in which the maximum W anomaly was approximately 0.9 mm, with a width of 12 km at the 0.5 mm value. The squall line moved from right to left and the average rainfall in the control ensemble was 14 mm. Close to the eastern edge of the humidity anomaly, rainfall was suppressed relative to the control (this was called the suppression area) by as much as 5 mm. As the squall moved further into the humid patch, rainfall was increased relative to the control (the enhancement area), with a peak enhancement of 12.5 mm in this case. Rainfall differences farther west reduced as the ensemble size increased and were considered to be ''noise.'' Humidity anomalies up to 89 km long were tested but the largest rainfall increase occurred when the anomaly was some 10–12 km long, as in Fig. 9a. These results were explained in terms of the effect of a horizontal gradient of humidity on the growth of convective cells in a multicellular squall line, represented schematically in Fig. 9b. As a squall line approaches an area of moist PBL air, the first cell that can ingest moist air (labeled 1 in Fig. 9b) develops rapidly because of enhanced latent heating. This cell expands and tends to reduce the mois-

ture supply to the previous cell (0), which is weakened. Movement of the cells relative to the ground means the rainfall enhancement in Fig. 9a is displaced to the west relative to the humidity anomaly. The combination of a weak cell followed by a strong cell generates a large rainfall gradient at the upstream edge of the humidity anomaly. A similar edge effect acts at the downstream edge of the patch: here a strong cell over the patch results in the first cell beyond the patch being weak. When the humidity anomaly is of the same length as the typical cell separation, approximately 10 km, a single cell over the patch benefits from two edge effects (i.e., cell 1 in Fig. 9b would be doubly enhanced), which explained why the largest rainfall response occurred at this length scale. These enhanced rainfall gradients across the edges of the humidity anomaly were consistent with the proposed feedback mechanism, insofar as the experiment could show.

These results were based on two-dimensional simulations and hence humidity anomalies were effectively infinite in the along-line direction. Given the importance of edge effects in these results, the present study used a three-dimensional model to perform similar simulations, set up as described in section 2c. As noted there, it was not possible to investigate the squall line's response to the variability modeled in section 4 because the model did not support a storm in that environment. PBL variability was represented by 1-km-deep humidity anomalies added ahead of the squall line. All anomalies were initially 8 km in the x direction (i.e., normal to the leading edge of the squall line) although diffusion and advection meant they were wider by the time the squall line arrived. The initial width of the anomaly in the y (along line) direction (L_y) was varied from 8 to 75 km, the latter meaning there was no along-line variability. The magnitude of the prescribed anomaly was altered so that the peak value of the W anomaly at the gust front was approximately 1 mm in all cases, similar to values used by Clark et al. (2003). This was larger than most of the PBL anomalies simulated in section 4 but was more likely to produce a clear response from the squall line, which was desirable in an exploratory study. The use of humidity anomalies without any temperature anomaly was justified by observations and by the results previously discussed and illustrated in Fig. 8a.

b. Results

Rainfall differences, relative to a control run, are summarized in Fig. 10. First we consider the case of no along-line variability (Fig. 10a), which is a 3D analogue of the 2D runs of Clark et al. (2003). In agreement with the earlier study, there was a zone of reduced rainfall near the upstream edge of the humidity anomaly, followed by an area of enhanced rainfall. The relatively large magnitude changes in the far west of the figure are thought likely to be noise, as was the case in 2D, but this could not be checked without ensembles. The average rainfall increase in the enhancement zone (defined as the contiguous points centered near $x = 20$ in Fig. 10a with an increase >0.5 mm) was 4.4 mm, compared with a control value of 9.8 mm. The largest point increase was more than 14 mm. These values were comparable to the 2D changes seen in Fig. 9a and again represented a substantial modification of the rainfall field.

Figure 10b shows that a humidity anomaly that initially had $L_y = 8$ km resulted in negligible rainfall suppression immediately upstream of the anomaly, with larger suppression now aligned with the enhancement in the along-line direction, slightly downstream of the humidity anomaly. The lack of upstream suppression was confirmed by runs in which the humidity anomaly was introduced at different (although nearby) x locations—all showed greater downstream suppression in the along-line direction. The peak rainfall increase is greater than 22 mm in Fig. 10b. An anomaly that was initially specified with $L_y = 16$ km produced a slightly weaker rainfall response (not shown), while anomalies of 24 and 32 km resulted in intermediate rainfall response (Figs. 10c and 10d), with along-line downstream suppression and moderate upstream suppression. The trend was thus for upstream suppression when the humidity anomaly had large L_y, moving to along-line downstream suppression and greater point rainfall increases for small L_y anomalies. In all cases the overall rainfall change was much greater than the extra moisture added via the humidity anomaly. Considering Fig. 10a as an example, when averaged over the area shown the rainfall change was 4.9 times larger than the added water, and in the vicinity of the anomaly this ratio was much larger. That the ratio exceeds one is the net result of several nonlinear processes that are involved in converting PBL humidity into surface rainfall.

Figure 11 summarizes these experiments by showing how the maximum point rainfall difference varied with L_y of the initial humidity anomaly. Values were only selected from y locations that were covered by the all humidity anomalies, namely, $y = 23$–33 in Fig. 10b. The maximum point change was largest for the anomaly with smallest L_y and decreased monotonically as L_y increased. The form of the response was similar for the maximum change over an area of 5 km $\times$ 5 km (not shown), with a rapid weakening of the response for larger L_y, although in this case the maximum was at 16 km. Although the along-line variability of the convection was relatively weak at this stage of the control runs compared with the later, fully 3D stage, variograms confirmed the visual impression (in plots of the control rainfall; not shown here) of an along-line correlation length for rainfall of approximately 12 km. It appears that the maximum rainfall response occurred when the along-line length scale of humidity variability was comparable to this natural length scale of the convection. Through extensive analysis, Clark et al. (2003) showed

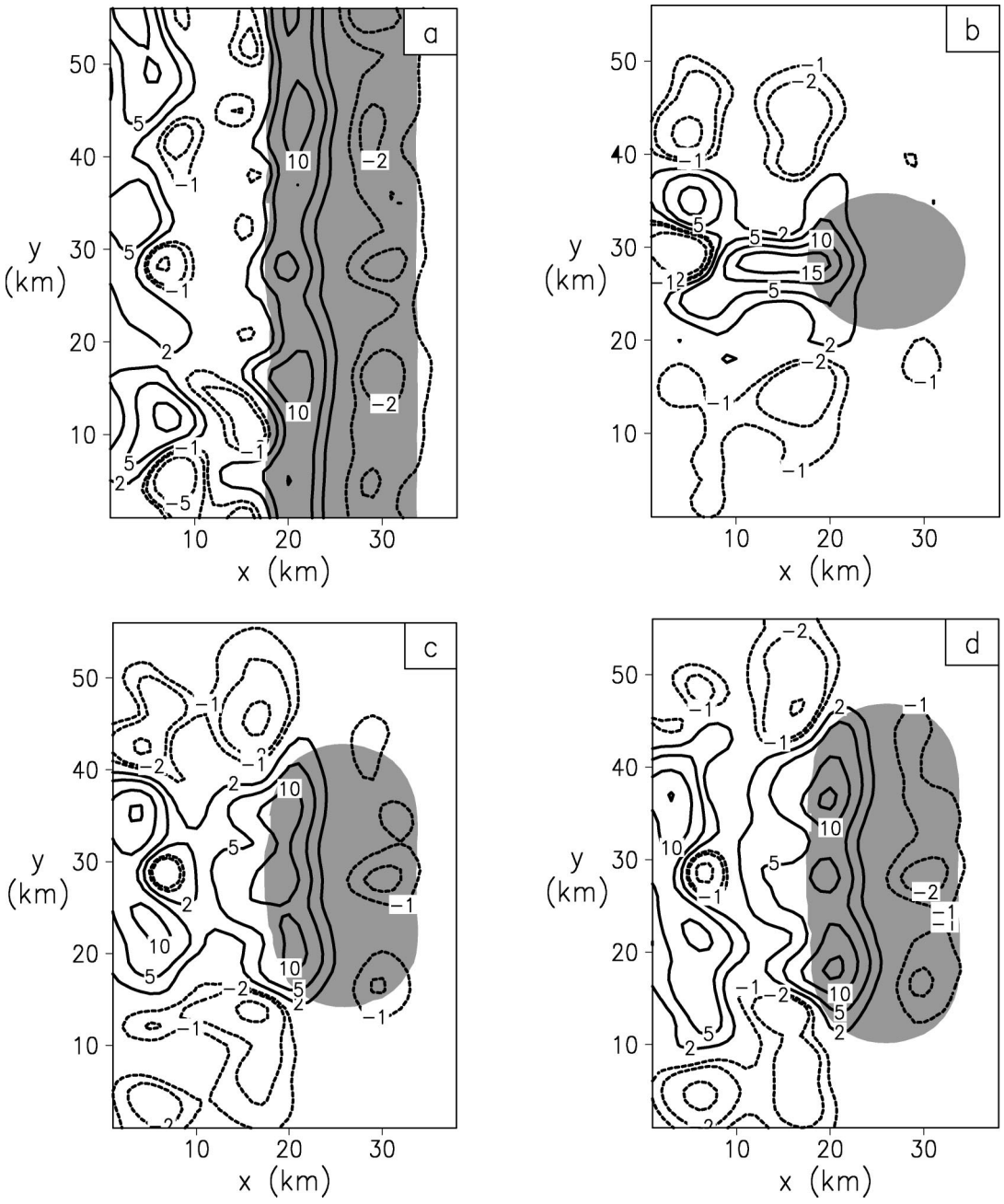

FIG. 10. Difference of rainfall (mm; contours) resulting from a prescribed difference of column precipitable water (mm; shaded) in three-dimensional simulations. The differences are relative to the control run, and the squall line moved from right to left. Rainfall contours are drawn at −5, −2, −1, 2, 5 mm and then every 5 mm. Precipitable water anomalies greater than 0.25 mm are shaded. The width of the precipitable water anomaly in the *y* direction is (a) infinite, (b) 8, (c) 24, and (d) 32 km.

that a similar result in 2D was explained by neighboring cells growing on a humidity gradient. The present work suggests that a similar process may be operating in the along-line direction too, although we stress that confirmation of this would require further work beyond this study.

These results from modeling of squall lines in two and three dimensions show that rainfall in such storms is sensitive to spatial variation of humidity in the PBL. Importantly, the rainfall response is sensitive to the length scale of the variability, with the strongest response at scales of some 10–15 km. By itself, this would favor a land surface–rainfall feedback at these relatively short scales.

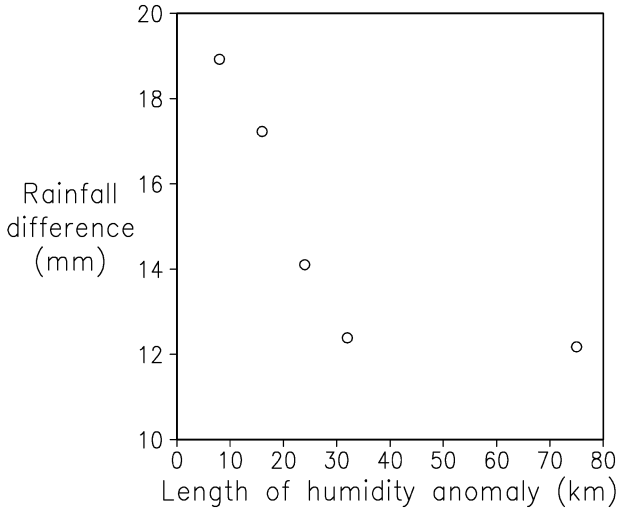

FIG. 11. Maximum point rainfall difference (mm) as a function of the length of the humidity anomaly (km) in the along-line direction.

6. Discussion and conclusions

A schematic of the proposed feedback process is shown in Fig. 12 and forms the basis for the following discussion. We start by assuming that the rainfall field from a storm has created strong spatial variability of soil moisture with a length scale of some 10–20 km (Fig. 12a). Features of this scale fit reasonably with a correlation length of approximately 30 km reported by Lebel and Le Barbé (1997) for event rainfall in the Sahel. In particular we consider an area of plentiful rainfall, surrounded by a relatively dry area. In a sparsely vegetated environment this will result in substantial spatial variability of surface fluxes of heat and moisture over the next 3–4 days. This variability is generally greater for sparser vegetation or initially drier soil, and less for dense vegetation or wetter soil.

While the pattern of surface variability persists it will tend to generate PBL variability. A plume of moist air is found over the wet surface feature and is displaced and elongated, particularly in the downwind direction (typically northeast in the Sahel, Fig. 12b). For the feedback to operate, the next rainfall event must occur while

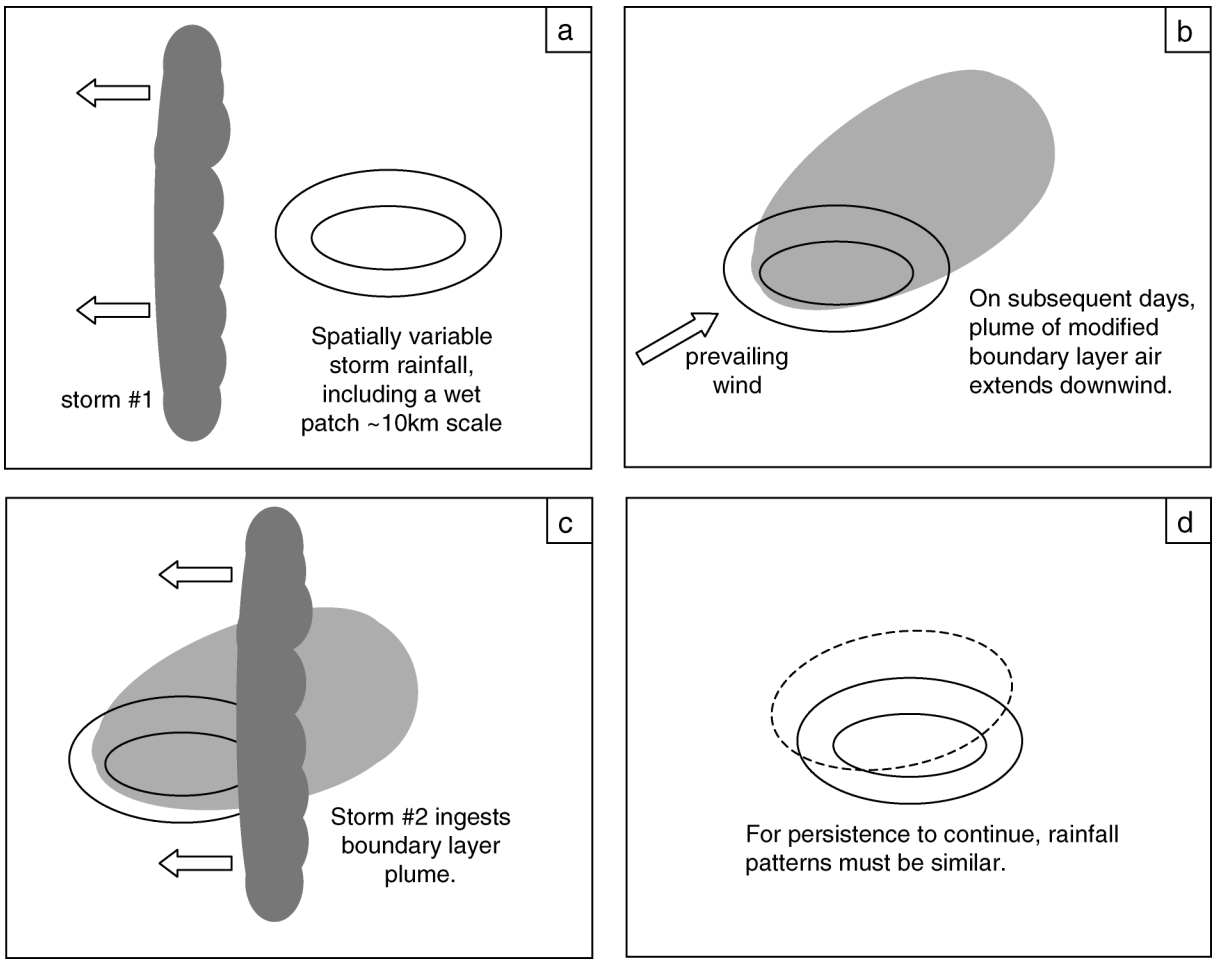

FIG. 12. (a)–(d) Schematic of the soil moisture–rainfall feedback.

there is still soil moisture (and hence PBL) variability. For typical Sahelian conditions this must be within 3–4 days or so, when bare soil evaporation is still relatively high in the wet patch but has tailed off in the drier areas. For a sandy soil, such as studied here, moisture drains quickly out of the surface layer, whereas a pattern of near-surface soil moisture would tend to persist longer in a less freely draining soil. The present study has only considered rainfall from large, organized squall lines, but rainfall may also come from other types of mesoscale systems or from isolated convection (e.g., a local thunderstorm). Such a local event would serve very well to first create a patch of wet soil.

If the PBL variability is sufficiently strong when the next storm arrives it may well affect the spatial distribution of rainfall from this storm (Fig. 12c). The time delay between the storm ingesting a PBL feature and the arrival of the associated rainfall at the surface, coupled with the motion of the storm relative to the ground, means that the PBL and rainfall features may be separated in space. Even given identical PBL anomalies, the rainfall response will vary between storms because of the large essentially stochastic element of convection. For example, a wet PBL patch may occur at the location where it can have maximum effect on the growth of a young convective cell and substantially increase the local rainfall. However, in another storm the same patch could be under the downdraft between cells and might then have negligible impact on the local rainfall. This is one way in which an established feedback might be broken, ending a period of rainfall persistence.

Finally, if the feedback is to persist beyond this storm the net result must be a rainfall field that shows similar patterns at similar locations to those from the first storm (Fig. 12d). The number of processes involved in the feedback and the degree of chance involved means that we do not expect an exact repetition. The squall-line modeling suggests that the surface rainfall response to PBL variability is displaced some 10 km or so in the direction of storm motion. In the Sahel, storms tend to travel westward, while the low-level monsoon winds during the wet season tend to come from the southwest. In terms of encouraging rainfall persistence over an area, it is interesting to speculate on the importance of the fact that that the low-level winds tend to advect a PBL anomaly to the east, while the delayed storm response tends to shift the rainfall back toward the surface anomaly. However, as speculated by Clark et al. (2003) it may be that the rainfall pattern is indeed displaced slightly downwind by each storm. The observations from HAPEX-Sahel (Fig. 1) show the broad pattern over several weeks, but the spatial resolution of the rain gauge network was insufficient to be able to observe any gradual downwind movement of the pattern from storm to storm.

A key question is, What controls the length scale of a soil moisture–rainfall feedback? As previous authors have pointed out, surface variability with length scales of some 10 km or less is more strongly countered by advection and diffusion than is variability on larger scales. Thus as far as the surface to boundary layer part of the proposed feedback is concerned, large space scales are favored. However, any feedback also depends upon the response of a storm to variability in the PBL. The results of squall-line modeling suggest that the convection shows a stronger response to relatively small-scale PBL variability, close to an inherent length scale of the convection itself. The combined surface–PBL–storm feedback might then be expected to be strongest at an intermediate length scale. Where this ''resonant'' length lies in relation to the component length scales depends upon how strongly each component process varies with length scale, for example, as seen in Figs. 6b and 11. In this way if the strength of a PBL anomaly is a relatively weak function of the length of the associated surface feature, but the rainfall-producing process strongly favors PBL anomalies on the length scale of the convective cells (say 10–20 km), there would be a strong preference for a land–atmosphere feedback on the 10–20-km scale. The fact that rainfall persistence was observed on convective length scales suggests that the convective processes exert a strong control on the scale of the overall feedback in the Sahel. Note that although the present study has concentrated on relatively small scales at which it was conventionally assumed that soil moisture–rainfall feedback was unlikely, this feedback could be embedded within any larger-scale interaction of the type described by previous authors.

The proposed feedback has implications in several fields. Soil hydrology and runoff are strongly affected by spatial variability of rainfall. Crop yields may vary substantially over relatively small distances if one area is persistently wetter. Local weather forecasts might need to take account of soil moisture–induced persistence. The dependence of the feedback mechanism on temporal and spatial details of convective cells represents a challenge to its incorporation in numerical weather prediction and regional climate models. For a grid-box length of some 10–50 km, moist convection is a parameterized, subgrid process, and it would be difficult to parameterize such a complicated feedback. As models move to higher spatial resolution, the problem moves to predicting the timing and location of individual cells. Deterministic forecasts of this are unlikely for the foreseeable future, if ever, given the likely sensitivity to initial conditions on small scales. More promisingly, an ensemble of forecasts could be used to determine the likelihood of a convective cell and a PBL anomaly interacting to give enhanced precipitation. Remote sensing techniques would be needed to describe the initial patterns of surface soil moisture and PBL humidity on sufficiently fine scales.

The persistent rainfall patterns found in observations by Taylor et al. (1997) and Taylor and Lebel (1998) offer compelling evidence for the previously unsuspected possibility of rainfall persistence at convective

scales, and a land–atmosphere feedback remains the most likely explanation. Further work would be beneficial in several areas. The response of the boundary layer to surface variability, particularly on length scales of tens of kilometers or less, and the importance of mesoscale circulations can be studied by numerical models. Three-dimensional large eddy simulations, in which a small grid-box length is used so that smaller eddies are resolved, may well be required to properly investigate the effect of surface variability on convective length scales. Further modeling is also required to better establish the sensitivity of squall lines to PBL variability. Observations are essential in assessing the realism of any modeling. As regards observing the feedback mechanism, in view of the ephemeral nature of the feedback and the relatively large spatial scales involved, remote sensing techniques are likely the only means by which the necessary surface, PBL, and rainfall characteristics could be monitored. The final steps in this work would be to use a fully coupled model to simulate all aspects of the soil moisture–rainfall feedback loop over several storms, to investigate whether rainfall persistence emerges and to examine the likelihood of such convective-scale persistence in other semiarid environments.

Acknowledgments. This work was supported financially by the Natural Environment Research Council under Grant GR3/11729. Most of the figures were prepared using GrADS. The authors thank all those who reviewed this work for their helpful comments.

REFERENCES

Avissar, R., and Y. Q. Liu, 1996: 3-dimensional numerical study of shallow convective clouds and precipitation induced by land-surface forcing. *J. Geophys. Res.,* **101,** 7499–7518.

Baker, R. D., B. H. Lynn, A. Boone, W. K. Tao, and J. Simpson, 2001: The influence of soil moisture, coastline curvature, and land-breeze circulations on sea-breeze-initiated precipitation. *J. Hydrometeor.,* **2,** 193–211.

Betts, A. K., and J. H. Ball, 1998: FIFE surface climate and site-average dataset 1987–89. *J. Atmos. Sci.,* **55,** 1091–1108.

Caniaux, G., J. L. Redelsperger, and J. P. Lafore, 1994: A numerical study of the stratiform region of a fast-moving squall line. Part I: General description and water and heat budgets. *J. Atmos. Sci.,* **51,** 2046–2074.

Chen, C., and W. R. Cotton, 1983: A one-dimensional simulation of the stratocumulus-capped mixed layer. *Bound.-Layer Meteor.,* **25,** 289–321.

Clark, D. B., C. M. Taylor, A. J. Thorpe, R. J. Harding, and M. E. Nicholls, 2003: The influence of spatial variability of boundary-layer moisture on tropical continental squall lines. *Quart. J. Roy. Meteor. Soc.,* **129,** 1101–1121.

D'Amato, N., and T. Lebel, 1998: On the characteristics of the rainfall events in the Sahel with a view to the analysis of climatic variability. *Int. J. Climatol.,* **18,** 955–974.

Delworth, T., and S. Manabe, 1989: The influence of soil wetness on near-surface atmospheric variability. *J. Climate,* **2,** 1447–1462.

Dolman, A. J., A. D. Culf, and P. Bessemoulin, 1997: Observations of boundary layer development during the HAPEX-Sahel intensive observation period. *J. Hydrol.,* **189,** 998–1016.

Emori, S., 1998: The interaction of cumulus convection with soil moisture distribution: An idealized simulation. *J. Geophys. Res.,* **103,** 8873–8884.

Fennessy, M. J., and J. Shukla, 1999: Impact of initial soil wetness on seasonal atmospheric prediction. *J. Climate,* **12,** 3167–3180.

Findell, K. L., and E. A. B. Eltahir, 1999: Analysis of the pathways relating soil moisture and subsequent rainfall in Illinois. *J. Geophys. Res.,* **104,** 31 565–31 574.

Goutorbe, J. P., and Coauthors, 1997: An overview of HAPEX-Sahel: A study in climate and desertification. *J. Hydrol.,* **189,** 4–17.

Houze, R. A., 1993: *Cloud Dynamics.* Academic Press, 573 pp.

Lebel, T., and L. Le Barbé, 1997: Rainfall monitoring during HAPEX-Sahel. 2. Point and areal estimation at the event and seasonal scales. *J. Hydrol.,* **189,** 97–122.

Lynn, B. H., W. K. Tao, and P. J. Wetzel, 1998: A study of landscape-generated deep moist convection. *Mon. Wea. Rev.,* **126,** 928–942.

McNider, R. T., and R. A. Pielke, 1981: Diurnal boundary-layer development over sloping terrain. *J. Atmos. Sci.,* **38,** 2198–2212.

Nicholls, M. E., and M. J. Weissbluth, 1988: A comparison of two-dimensional and quasi-3-dimensional simulations of a tropical squall line. *Mon. Wea. Rev.,* **116,** 2437–2452.

Pal, J. S., and E. A. B. Eltahir, 2001: Pathways relating soil moisture conditions to future summer rainfall within a model of the land–atmosphere system. *J. Climate,* **14,** 1227–1242.

Pielke, R. A., and Coauthors, 1992: A comprehensive meteorological modeling system—RAMS. *Meteor. Atmos. Phys.,* **49,** 69–91.

Raupach, M. R., 1991: Vegetation–atmosphere interaction in homogeneous and heterogeneous terrain—Some implications of mixed-layer dynamics. *Vegetatio,* **91,** 105–120.

Redelsperger, J. L., and J. P. Lafore, 1988: A 3-dimensional simulation of a tropical squall line–convective organization and thermodynamic vertical transport. *J. Atmos. Sci.,* **45,** 1334–1356.

——, and Coauthors, 2000: A GCSS model intercomparison for a tropical squall line observed during TOGA-COARE. I: Cloud-resolving models. *Quart. J. Roy. Meteor. Soc.,* **126,** 823–863.

Roux, F., J. Testud, M. Payen, and B. Pinty, 1984: West-African squall-line thermodynamic structure retrieved from dual-doppler radar observations. *J. Atmos. Sci.,* **41,** 3104–3121.

Shukla, J., and Y. Mintz, 1982: Influence of land-surface evapo-transpiration on the earth's climate. *Science,* **215,** 1498–1501.

Shuttleworth, W. J., 1988: Macrohydrology—The new challenge for process hydrology. *J. Hydrol.,* **100,** 31–56.

Taylor, C. M., 2000: The influence of antecedent rainfall on Sahelian surface evaporation. *Hydrol. Processes,* **14,** 1245–1259.

——, and T. Lebel, 1998: Observational evidence of persistent convective-scale rainfall patterns. *Mon. Wea. Rev.,* **126,** 1597–1607.

——, F. Saïd, and T. Lebel, 1997: Interactions between the land surface and mesoscale rainfall variability during HAPEX-Sahel. *Mon. Wea. Rev.,* **125,** 2211–2227.

Walko, R. L., W. R. Cotton, M. P. Meyers, and J. Y. Harrington, 1995: New RAMS cloud microphysics parameterization. 1. The single-moment scheme. *Atmos. Res.,* **38,** 29–62.

——, and Coauthors, 2000: Coupled atmosphere–biophysics–hydrology models for environmental modeling. *J. Appl. Meteor.,* **39,** 931–944.

Weisman, M. L., J. B. Klemp, and R. Rotunno, 1988: Structure and evolution of numerically simulated squall lines. *J. Atmos. Sci.,* **45,** 1990–2013.

Zeng, N., J. D. Neelin, K. M. Lau, and C. J. Tucker, 1999: Enhancement of interdecadal climate variability in the Sahel by vegetation interaction. *Science,* **286,** 1537–1540.